

Journal of Materials Chemistry A

Accepted Manuscript



This is an *Accepted Manuscript*, which has been through the Royal Society of Chemistry peer review process and has been accepted for publication.

Accepted Manuscripts are published online shortly after acceptance, before technical editing, formatting and proof reading. Using this free service, authors can make their results available to the community, in citable form, before we publish the edited article. We will replace this *Accepted Manuscript* with the edited and formatted *Advance Article* as soon as it is available.

You can find more information about *Accepted Manuscripts* in the [Information for Authors](#).

Please note that technical editing may introduce minor changes to the text and/or graphics, which may alter content. The journal's standard [Terms & Conditions](#) and the [Ethical guidelines](#) still apply. In no event shall the Royal Society of Chemistry be held responsible for any errors or omissions in this *Accepted Manuscript* or any consequences arising from the use of any information it contains.

High Efficiency All-Polymer Solar Cells Realized by Synergistic Effect between Polymer Side-Chain Structure and Solvent Additive

Jianyu Yuan, Wanli Ma*

Institute of Functional Nano & Soft Materials (FUNSOM), Jiangsu Key Laboratory for Carbon-Based Functional Materials & Devices, Collaborative Innovation Center of Suzhou Nano Science and Technology, Soochow University

E-mail: wlma@suda.edu.cn

Keywords: all-polymer solar cells, π -conjugated side-chain, solvent additive, blend morphology, synergistic effect

Abstract: By adopting a series of donor-acceptor (D-A) polymers containing Benzo[1,2-b:4,5-b']dithiophene (BDT) and thieno[3,4-c]pyrrole-4,6-dione (TPD) with different number of alkyl aromatic side-chains, we demonstrating a high optimized PCE of 4.35% for all-polymer solar cells by incorporating an n-type polymer N2200. Through systematic characterization of tapping mode atomic force microscopy (AFM), 2-demissonal grazing-incidence X-ray diffraction (2d-GIXD), photoluminescence spectra and peak force-kelvin probe force microscopy (PF-KPFM), we have shown that the introduction of alkyl aromatic side chains to donor polymer backbone is beneficial for the intermolecular π - π stacking and hence improves polymer crystallinity as well as hole mobility. More importantly, we discovered that conjugated side-chains and additive can work synergistically to restore the intermolecular stacking of donor/acceptor polymers in the as-cast amorphous blend film and meanwhile develop fine phase segregation for efficient exciton dissociation

and transport. As a result, the donor polymer PTP8 with fully alkyl aromatic side chains demonstrated an improved short-circuit current density (J_{sc}), a high open-circuit voltage (V_{oc}) of ~ 1.00 V and a power conversion efficiency (PCE) of 4.35 % after the addition of 0.5% DIO, which is among the highest reported efficiencies for all polymer solar cells.

1. Introduction

Solution-processed polymer/fullerene solar cells (PSCs) have attracted tremendous interest in the past decade because of their advantages like light-weight, mechanical flexibility and semi-transparency.¹ However, fullerene derivatives demonstrate weak absorbance in the visible region and tendency to aggregation under elevated temperatures, leading to inefficient photon harvest as well as deteriorated blend morphology and consequently reduced lifetime of PSCs.² By replacing fullerene with an electron-accepting polymer, all-polymer solar cells can avoid the drawbacks of fullerenes such as tedious purification, chemical and electronic diversities³ along with limited light absorption and poor thermal stability.

All-polymer photovoltaic devices, in which the active layer is composed of both an electron-donating polymer and an electron-accepting polymer, have lagged significantly behind polymer/fullerene system in development and performance.^{3d} Fortunately, the latest endeavors in selecting new donor/acceptor polymers and improving device fabrication process have boost the power conversion efficiency (PCE) of all-polymer devices to over 4%,⁴⁻⁵ Quite recently, Ito et al.^{5a} have reported a

record efficiency of 5.7% by carefully choosing an efficient donor/acceptor (D/A) polymer pair. On the other hand, the development none-fullerene solar cells based on small molecule acceptors have boosted the efficiency to over 6%.^{3e-f} Among the polymer acceptors exploited so far, naphthalene- and perylene tetracarboxylic diimide (NDI and PDI)-based derivatives are the most frequently reported ones due to their simple synthesis, easy-to-tune energy levels, and relatively high electron mobilities.⁶ The efforts to achieve high performance all-polymer solar cells were thus mainly focused on improvement of device processing condition and selection of donor polymers to obtain optimal miscibility, morphology, energy level alignment and balanced carrier mobility.^{4,5} The current device performance is believed to be hindered by limited charge separation or charge transport in the all-polymer film, depending on the specific polymer D/A combination. Thus to further improve the device performance, the effect of polymer structures and processing conditions on the device morphology and performance should be investigated and a more general designing approach would be desired to obtain ideal donor-polymer.

In this contribution, a series of low band-gap donor polymers (P8, PT8, PTP8) sharing the same backbone were used together with poly{[*N,N'*-bis(2-octyldodecyl)-naphthalene-1,4,5,8-bis(dicarboximide)-2,6-diyl]-*alt*-5,5'-(2,2'-bithiophene)}[P(NDI2OD-T2)]; Polyera ActivInk N2200] in all-polymer solar cells. As shown in **Scheme 1**, P8 has flexible side chains on both donor and acceptor comonomers. PT8 has conjugated side chains appended to the donor comonomer while both alkyl aromatic side chains for PTP8. The correlation between side chain

structure and device performance was systematically studied. We reported high open circuit voltage ($V_{oc} = \sim 1.0$ V) and PCE of 4.35% for PTP8 device after the addition of 0.5% (v/v) 1,8-diiodooctane (DIO), which is among the highest reported efficiencies for all-polymer PSCs. We found that the introduction of conjugated side chain can enhance polymer intermolecular π - π interaction as well as crystallinity and may improve the effect of solvent additives, leading to improved morphology and carrier transport in all-polymer blend, as proved by 2-dimensional grazing incidence x-ray diffraction (2D-GIXD). We also show that the surface condition can be adjusted by solvent additive by using kelvin probe force microscopy (KPFM) characterization. Our results suggest that the synergistic effect between polymer side-chain and solvent additive is critical for the device improvement, which may become a general and effective approach to enhance the performance of current all-polymer solar cells.

2. Experimental Section

2.1 General:

UV-vis-NIR spectra were recorded on a Perkin Elmer model Lambda 750. Photoluminescence spectra were recorded on a Horiba Jobin Yvon model FL-TCSPC. Tapping-mode AFM images were obtained with a Veeco Multimode V instrument, 2-D GIXD experiments were conducted at Shanghai Synchrotron Radiation Facility (SSRF) on diffraction beam line (BL14B1). PF-KPFM measurements were performed with a Burkert Dimension Icon instrument. NDI2OD-Br2 and 2,5-bis(trimethylstannyl)-thieno-[3,2-b]-thiophene were purchased from Sunatech Inc.

tri(*o*-tolyl)phosphine and Pd₂(dba)₃ were purchased from Strem Chemicals Inc. Toluene and DMF were purchased from Adamas Reagent. Ltd and distilled before use.

2.2 Synthesis of polymers N2200:

N2200 was synthesized according to the procedures as follows: in a 50 mL reaction tube, NDI2OD-Br₂ (200 mg, 0.21 mmol), 2,5-bis(trimethylstannyl)-thieno-[3,2-*b*]-thiophene (95 mg, 0.21 mmol), tri(*o*-tolyl)phosphine (0.02 g, 0.08 mmol), and Pd₂(dba)₃ (0.01 g, 0.01 mmol) were dissolved in 5 mL dry toluene and 0.5 mL DMF under argon. After stirred at 110 °C for 4 days, the mixture was cooled to room temperatures and precipitated in methanol (80 mL). The precipitate was filtered and washed with acetone (24 h) and hexane (24 h) successively in a soxhlet apparatus to remove oligomers and catalyst residue. Finally, the polymer was extracted with chloroform (6 h). The chloroform fraction was concentrated and precipitated in methanol. The precipitate was filtered and dried in vacuum at 80 °C overnight. GPC: $M_n = 36.0 \text{ kg mol}^{-1}$, PDI = 2.5.

2.3 Device Fabrication and Testing:

Polymer solar cells were fabricated with a general structure of ITO/PEDOT-PSS (40 nm)/polymer:N2200/LiF/Al. Patterned ITO glass substrates were cleaned by sequential ultrasonic treatment in detergent, acetone, deionized water and isopropyl alcohol. The organic residue was further removed by treating with UV-ozone for 10 min. A thin film of PEDOT: PSS (~40 nm) was spin-coated on ITO substrates and dried at 150 °C for 10 min. A blend of polymers with different ratios was dissolved in

chloroform or chloroform containing 0-5% (v/v) diiodooctane, spin-coated at varying speed (1000-3500 rpm) for 40 s, 0.6 nm of LiF (0.1Å/s) and 100 nm Al (2Å/s) layers were then thermally evaporated on the active layer at a pressure of 1.0×10^{-6} mbar through a shadow mask (active area 7.25 mm²). The current density–voltage characteristics of the photovoltaic cells were measured using a Keithley 2400 (*I–V*) digital source meter under a simulated AM 1.5G solar irradiation at 100 mW/cm² (Newport, Class AAA solar simulator, 94023A-U). The light intensity is calibrated by a certified Oriel Reference Cell (91150V) and verified with a NREL calibrated Hamamatsu S1787-04 diode. The external quantum efficiency (EQE) was performed using a certified IPCE equipment (Zolix Instruments, Inc, SolarCellScan100).

3. Results and Discussion

3.1. Polymers Synthesis and Properties

The donor polymer P8, PT8 and PTP8 was synthesized following our previous report.⁷ N2200 was synthesized using an improved procedure⁸ as described in the experimental section. The molecular structures and energy levels of donor and acceptor polymer are shown in **Scheme 1**. Despite the modification of side-chains, the LUMO (lowest unoccupied molecular orbital) and HOMO (highest occupied molecular orbital) levels of the donor polymers are all around -3.60 eV and -5.50 eV respectively,^{7b} which help to form type II structure with the acceptor polymer N2200, as well as achieve high open circuit voltage (V_{oc}). The normalized film absorption spectra of the adopted polymers are shown in **Figure 1**. The donor polymers exhibit

similar absorption and a bandgap around 1.8 eV, likely due to their BDT-TPD based backbone structure. The absorption of N2200 is broader and the donor/acceptor blend absorption can be extended to over 900 nm, consequently increasing the photon harvested by the all-polymer photovoltaic devices.

3.2. All-Polymer Solar Cells Performance

All-polymer devices were fabricated with the conventional architecture of ITO/PEDOT-PSS(40 nm)/Polymer:N2200/LiF(0.6 nm)/Al(100 nm), as shown in **Figure 2a**. Throughout the experiment, a fixed D/A polymer concentration of 12 mg/mL was adopted, with chloroform used as the optimal processing solvent. The device optimizations include fine adjustment of film thickness, blend ratio (Tables S1) and additive concentration (**Table 1**). 1,8-diiodooctane (DIO) was used in this work to improve film morphology,⁹ which has been proven to be an efficient additive in polymer-fullerene as well as in none-fullerene solar cells.^{4a,6b} The J - V characteristics of the optimized devices for different donor polymers are shown in **Figure 2**, with the detailed parameters listed in Table S2. All the devices exhibit high V_{oc} around 1.00 V. And optimized PCEs of 1.52%, 1.75% and 4.35% are achieved for P8, PT8 and PTP8, respectively. The PCE difference can mainly be ascribed to their different J_{sc} and FF. The mobility of polymer:N2200 blend film was measured by using space charge limited current (SCLC) technique.¹⁰ A device structure of ITO//PEDOT-PSS(40 nm)/Polymer:N2200/MoOx (6 nm)/Al (100 nm) was adopted and the results are shown in Figure S1. The calculated hole mobility is $6.12 \times 10^{-6} \text{ cm}^2 \text{V}^{-1} \text{s}^{-1}$, $7.52 \times 10^{-6} \text{ cm}^2 \text{V}^{-1} \text{s}^{-1}$, and $4.78 \times 10^{-5} \text{ cm}^2 \text{V}^{-1} \text{s}^{-1}$ for the film of P8:N2200, PT8:N220 and

PTP8:N2200 respectively, which is accordance with their FF. The higher mobility of PTP8 and PT8 compared to P8 can be ascribed to their enhanced intermolecular packing assisted by alkyl aromatic side-chains. As shown in **Figure 3**, the photoluminescence of all three donor polymers are effectively quenched by the acceptor polymer. The lifetime of excited excitons are also apparently reduced when blending with N2200, which suggests exciton dissociation process at the donor/acceptor interface. We observe that the addition of 0.5% (v/v) DIO can further reduce the exciton lifetime of all the blend films while the effect is more significant for polymers PT8 and PTP8 with conjugated side chains. This result is consistent with the observation that PTP8 and PT8 based devices have much more improvement than P8 based devices after using DIO, as shown in Table S2. It is worth noting that the addition of 2% DIO results in less efficient exciton separation, likely due to deteriorated morphology. We further studied the effect of DIO on the PTP8:N2200 based photovoltaic devices in detail, as shown in the **Figure 4** and **Table 1**. The devices cast from pure chloroform solution exhibit a maximum PCE of 2.83 % with a J_{sc} of 6.53 mA/cm², a V_{oc} of 0.975 V, and a FF of 44.4%. After the addition of 0.5% (v/v) DIO, the devices achieve a significantly higher J_{sc} of 8.43 mA/cm², a FF of 52.8% and a PCE of 4.35%. The improved morphology (Figure S2) and increased film absorbance after using DIO (**Figure 5**) may account for the enhanced performance. Further increasing the amount of solvent additive, however, results in gradual decrease of the device performance. PCEs of 3.88%, 3.27%, 2.82% and 1.64% were achieved for devices using 1.0%, 2.0%, 3.0% and 5.0% (v/v) DIO respectively. We

also evaluated the forming of carrier pathways at different DIO concentrations. The carrier mobility of PTP8:N2200 blend film was measured by using space charge limited current (SCLC) technique,¹⁰ with the results shown in Figure S3 and Table S3. With increased additive concentration, a gradual decrease in both the electron and hole mobility is observed, indicating unfavorable morphology for carrier transport in the all-polymer film. The electron and hole mobility is high and balanced with 0.5% DIO which is consistent with the optimal FF at this processing condition. To evaluate the photo-response of PTP8 based devices and calibrate the J_{sc} data, external quantum efficiencies (EQE) of optimized devices with or without DIO was measured and shown in **Figure 5**. After using DIO, the film absorbance and EQE are both enhanced. The devices show relatively high photo-conversion efficiency over the whole wavelength range (300-850 nm). Judged by the pick positions, we conclude that the increased absorption and current is mainly contributed by PTP8, likely due to improved packing by using DIO. However, N2200 also contributes to the EQE improvement in the 700-900 nm regions, suggesting overall enhancement of charge separation and transport in the blend film after using DIO. It is worth noting that the J_{sc} calculated by integrating the EQE curve with an AM1.5G reference spectrum is within ~3% error compared to the corresponding J_{sc} obtained from the $J-V$ curves.

3.3 All-Polymer Blend Morphology

The surface morphology of the polymer:N2200 film with or without DIO was carefully investigated to understand the effect of additive by using tapping mode atomic force microscopy (AFM). As shown in Figure 6, before the use of DIO,

PTP8 and PT8 blend films have more pronounced polymer aggregation structures compared to the relatively uniform film of P8, which may arise from the enhanced molecular packing assisted by conjugated side chains. After the addition of 0.5% (v/v) DIO, the domains of the two polymers in PTP8:N2200 film are more uniformly distributed, which may lead to enhanced exciton dissociation and is in accordance with the dramatically enhanced device performance and photoluminescence quenching after using DIO. The effect of DIO concentration on morphology was further studied. As shown in Figure S2, increasing the amount of DIO from 0.5%, 1.0%, 2.0% to 3.0% for the PTP8:N2200 blend results in gradually increased surface roughness and domain sizes, leading to enhanced phase aggregation with a scale too large to effectively separate excitons. The observation is also consistent with the low device performance.

We also investigated the surface potentials of the blend films w/wo DIO by using the Peak Force-Kelvin Probe Force Microscopy (PF-KPFM).¹¹ KPFM measures contact potential difference between the tip and the blend film. The PF-KPFM surface potential images and the corresponding analysis curves of contact potential differences are shown in Figure 7. According to the PF-KPFM measurements, the average contact surface potentials of the blend film casted from pure chloroform is found to be ~ 0.3 V and ~ 0.2 V higher than that of the films with 0.5% and 2.0% DIO additive, respectively. Thus the addition of DIO can substantially change the film surface condition and lower the surface potential of the organic/metal interface. Compared to the blend film without additive, the addition of 0.5% DIO dramatically

reduces the vacuum level (VL) of the cathode side by ~ 0.3 V and also leads to more uniform distribution of surface potential, which may improve the electron extraction at the polymer/Al interface and result in enhanced device performance.^{11a}

3.4 Molecular Packing in All-Polymer Bulk Heterojunction Blend

To gain insight into the mechanism of device improvement by introducing alkyl aromatic side-chains and additive, we further performed very detailed 2d-GIXD to reveal the corresponding bulk morphology change. In the scattering spectra of pristine PT8, PTP8 (Figure S4) and N2200 (**Figure 8**), the (010) peak corresponding to π - π stacking is more pronounced in the out-of-plane direction, which suggests that majority of the polymer backbones are oriented parallel to the substrates,¹² which is favorable for carrier transport cross the film to the electrode. The evidently stronger (010) peak of PTP8 and PT8 compared to P8 indicates enhanced intermolecular packing likely resulting from introduced conjugated side-chains. Note that N2200 also shows evident (100) and (200) peak in the in-plane direction. The GIXD patterns of polymer:N2200 blend films cast from chloroform without DIO are also shown in Figure S6. We observe the weakening of (010) peaks for all polymer blends, suggesting the amorphous nature of the as-cast polymer blend film. After the addition of 0.5% DIO, however, the (010) peaks of PTP8 and PT8 is restored, while the scattering rings of P8 blend are almost not enhanced. Thus we speculate that PTP8 and PT8 with conjugated side-chains can more effectively recover their intermolecular π - π stacking and carrier mobility with the aid of DIO, while P8 with alkyl side chains has smaller conjugation area and less coplanarity, demonstrating

weaker capability to restore intermolecular packing when using DIO. If we watch carefully, we can see that the (010) peak in PT8 blend is slightly stronger than that of PTP8 blend, which is actually in accordance with its AFM image in **Figure 6**. It is worth noting that the (100) and (200) peak of N2200 can be observed in PTP8 and PT8 blends. It indicates that N2200 can basically retain its order when blending with these two polymers, which is beneficial for maintaining efficient electron transport. Furthermore, we investigate the morphology evolution of PTP8 blend with increased DIO content (0-5 %) (**Figure 8**). The (100) peaks of both PTP8 and N2200 in the blend film exhibit no shift before and after the addition of DIO, indicating that no intercalated phases are formed in the PTP8:N2200 film.¹³ Without using DIO, the halo around 1.5 \AA^{-1} corresponding to the polymer (010) peaks is very weak for the blend film. The peak is becoming more prominent with increased DIO concentration and reaches the maximum intensity at 0.5% (v/v) DIO. The (100) and (200) peaks of N2200 are also largely enhanced at a DIO concentration between 0.5% to 2%, with the maximum peak intensity and electron mobility obtained at about 1% DIO. The results suggest that the DIO concentration may impact the donor and acceptor polymer differently which requires further study to understand the mechanism. In **Figure 9**, the one dimension line-cuts of both XY and Z axis were presented, t exhibited a DIO concentration-dependent diffraction intensity change for both the donor and the acceptor polymers, apparently, the all-polymer blend with the addition of 0.5% DIO demonstrated more pronounced diffraction peaks in both directions, and at higher DIO concentration, decreased diffraction intensity were witnessed from both

two axis. As a result, improved intermolecular packing for both donor and acceptor polymers can be achieved at 0.5 % DIO. Consequently, balanced carrier transport and optimal efficiency are demonstrated. At higher DIO loadings, the (010) peak is gradually diminished. And all scattering peaks nearly disappear at a very high DIO concentration of 5%, indicating a totally amorphous blend film, which is in accordance with the relatively low efficiency and carrier mobility for devices with high concentration DIO.

4. Conclusions

By introducing different number of alkyl aromatic side chains to the donor polymers, the performance of all-polymer PSCs was greatly improved and an optimized PCE of 4.35% was obtained after the addition of 0.5% DIO, which is among the highest reported efficiencies for all polymer PSCs. The effect of alkyl aromatic side chains and solvent additive on the device morphology and performance was systematically studied. The introduction of conjugated side chains is beneficial to the intermolecular π - π stacking and hence improves polymer crystallinity as well as hole mobility. More importantly, we discovered that conjugated side-chains and DIO can work synergistically to restore the intermolecular stacking of donor/acceptor polymers in the as-cast amorphous blend film and meanwhile develop fine phase segregation for efficient exciton dissociation and transport. Although higher PCEs for all-polymer PSCs have been reported, our work may propose a more universal and

facile designing method to tailor existing polymers to achieve improved performance in all-polymer photovoltaic devices

Acknowledgements

We acknowledge technical support from workers at Shanghai Synchrotron Radiation Facility (SSRF) on diffraction beamline (BL14B1). We appreciate *Prof.* Lifeng Chi for helpful PF-KPFM characterization. This work was supported by the National High Technology Research and Development Program of China (863 Program) (Grant No. 2011AA050520), the National Natural Science Foundation of China (Grant No. 61176054), the Natural Science Foundation of Jiangsu Province, China (Grant No. BK2011279), the Doctoral Fund of Ministry of Education of China (Grant No. 20113201120019). J. Yuan thanks State-Sponsored Scholarship for Graduate Students from China Scholarship Council and the Innovation of Graduate Student Training Project in Jiangsu Province.

References

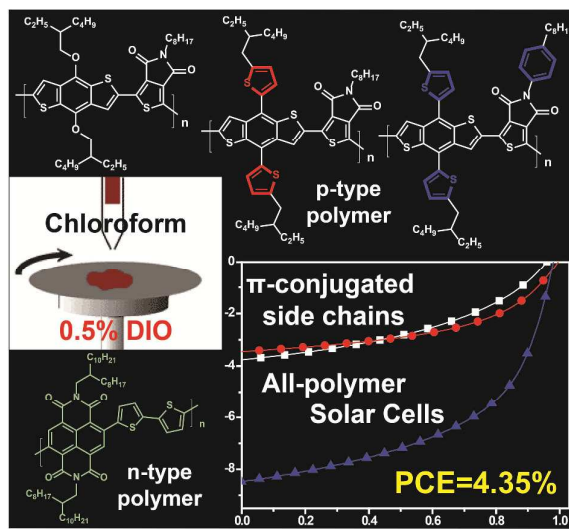
- [1] a) Y.-J. Cheng, S.-H. Yang, C.-S. Hsu, *Chem. Rev.* 2009, 109, 5868; b) Y. F. Li, *Acc. Chem. Res.* 2012, **45**, 723. c) L. Dou, J. You, J. Yang, C.-C. Chen, Y. He, S. Murase, T. Moriarty, K. Emery, G. Li, Y. Yang, *Nat. Photonics*, 2012, **6**, 180; d) J. You, L. Dou, K. Yoshimura, T. Kato, K. Ohya, T. Moriarty, K. Emery, C.-C. Chen, J. Gao, G. Li, Y. Yang, *Nat. Commun.* 2013, **4**, 1446. e) J.-D. Chen, C. Cui, Y.-Q. Li, L. Zhou, Q.-D. Ou, C. Li, Y. Li, J.-X. Tang, *Adv. Mater.* DOI:

- 10.1002/adma.201404535; f) Y. Liu, J. Zhao, Z. Li, C. Mu, W. Ma, H. Hu, K. Jiang, H. Lin, H. Ade, H. Yan, *Nat. Commun.* DOI:10.1038/ncomms6293.
- [2] a) J. M. Warman, M. P. de Haas, T. D. Anthopoulos, D. M. de Leeuw, *Adv. Mater.* 2006, **18**, 2294; b) W. Y. Huang, P. T. Huang, Y. K. Han, C. C. Lee, T. L. Hsieh, M. Y. Chang, *Macromolecules* 2008, **41**, 7485; c) T. Agostinelli, S. Lilliu, J. G. Labram, M. C. Quiles, M. Hampton, E. Pires, J. Rawle, O. Bikondoa, D. D. C. Bradley, T. D. Anthopoulos, J. Nelson, J. E. Macdonald, *Adv. Funct. Mater.* 2011, **21**, 1701.
- [3] a) X. Zhan, Z. Tan, B. Domercq, Z. An, X. Zhang, S. Barlow, Y. Li, D. Zhu, B. Kippelen, S. R. Marder, *J. Am. Chem. Soc.* 2007, **129**, 7246; b) M. C. Scharber, D. Mühlbacher, M. Koppe, P. Denk, C. Waldauf, A. J. Heeger, C. J. Brabec, *Adv. Mater.* 2006, **18**, 789; c) J. D. Servaites, B. M. Savoie, J. B. Brink, T. J. Marks, M. A. Ratner, *Energy Environ. Sci.* 2012, **5**, 8343; d) A. Facchetti, *Mater. Today* 2013, **16**, 123; e) Y. Lin X. Zhan *Mater. Horiz.* 2014, **1**, 470; f) J. Zhao, Y. Li, H. Li, Y. Liu, K. Jiang, C. Mu, T. Ma, J. Y. L. Lai, H. Hu, D. Yu, H. Yan, *Energy Environ. Sci.* DOI: 10.1039/C4EE02990A ; f) X. Zhan, A. Facchetti, S. Barlow, T. J. Marks, M. A. Ratner, M. R. Wasielewski, S. R. Marder, *Adv. Mater.* 2011, **23**, 268
- [4] a) E. Zhou, J. Cong, K. Hashimoto, K. Tajima, *Adv. Mater.* 2013, **25**, 6991; b) D. Mori, H. Benten, I. Okada, H. Ohkita, S. Ito, *Adv. Energ. Mater.* 2013, **4**, 1301006; c) Y. Zhou, T. Kurosawa, W. Ma, Y. Guo, L. Fang, K. Vandewal, Y. Diao, C. Wang, Q. Yan, J. Reinspach, J. Mei, A. L. Appleton, G. I. Koleilat, Y.

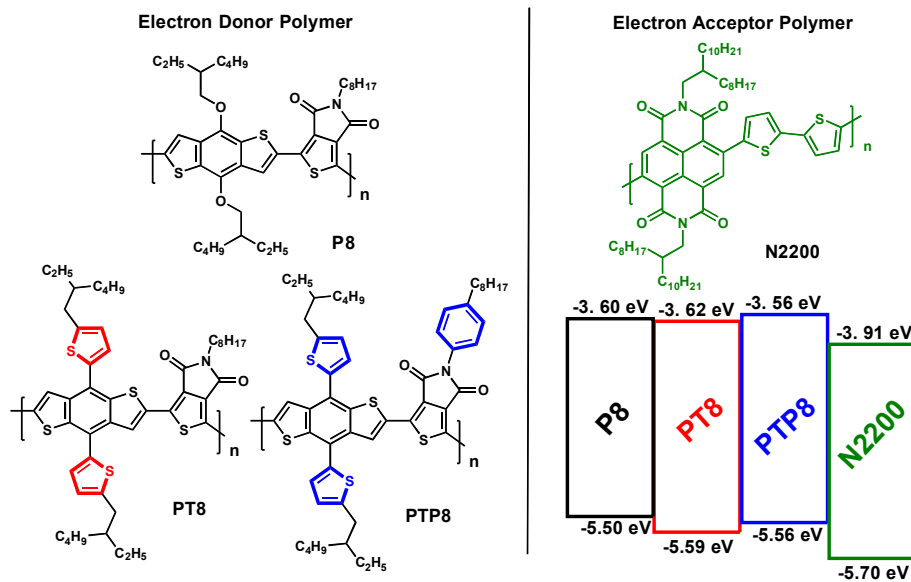
- Gao, S. C. B. Mannsfeld, A. Salleo, H. Ade , D. Zhao, Z. Bao, *Adv. Mater.* 2014, **26**, 3767; d) T. Earmme, Y. -J. Hwang, S. Subramaniyan, S. A. Jenekhe, *Adv.Mater.* 2014, **26**, 6080; e) Y. Lin, Z.-G. Zhang, H. Bai, J. Wang, Y. Yao, Y. Li, D. Zhu, X. Zhan, *Energy Environ. Sci.* 2014, DOI: 10.1039/c4ee03424d; f) Y. Lin, J. Wang, Z. Zhang, H. Bai, Y. Li, D. Zhu, X. Zhan, *Adv. Mater.* 2015, DOI: 10.1002/adma.201404317.
- [5] a) D. Mori, H. Benten, I. Okada , H. Ohkita, S. Ito, *Energy Environ. Sci.* 2014, **7**, 2939; b) C. Mu, P. Liu, W. Ma, K. Jiang¹, J. Zhao¹, K. Zhang, Z. Chen, Z. Wei¹, Y. Yi, J. Wang, S. Yang, F. Huang, A. Facchetti, H. Ade He Yan, *Adv. Mater.* 2014, **26**, 7224; c) K. D. Deshmukh, T. Qin, J. K. Gallaher, A. C. Y. Liu, E. Gann, K. O'Donnell, L. Thomsen, J. M. Hodgkiss, S. E. Watkins, C. R. McNeill, *Energy Environ. Sci.* 2015, **8**, 332.
- [6] a) H. Yan, Z. H. Chen, Y. Zheng, C. Newman, J. R. Quinn, F. Dötz, M. Kastler, A. Facchetti, *Nature* 2009, **457**, 679; b) E. J. Zhou, J. Z. Cong, Q. S. Wei, K. Tajima, C. H. Yang, K. Hashimoto, *Angew. Chem. Int. Ed.* 2011, **50**, 2799; c) T. Earmme, Y. -J. Hwang, N. M. Murari, S. Subramaniyan, S. A. Jenekhe, *J. Am. Chem. Soc.* 2013, **135**, 14960; d) P. Cheng, L. Ye, X. Zhao, J. Hou, Y. Li, X. Zhan, *Energy Environ. Sci.* 2014, **7**, 1351.
- [7] a) J. Yuan, Z. Zhai, H. Dong, J. Li, Z. Jiang, Y. Li, W. Ma, *Adv. Funct. Mater.*, 2013, **23**, 885; b) J. Yuan, H. Dong, M. Li, X. Huang, J. Zhong, Y. Li, W. Ma, *Adv. Mater.* 2014, **26**, 3624.
- [8] a) H. Chen, Y. Guo, Z. Mao, G. Yu, J. Huang, Y. Zhao, Y. Liu, *Chem. Mater.*

- 2013, **25**, 3589; b) A. Luzio, D. Fazzi, D. Natali, E. Giussani, K. –J. Baeg, Z. Chen, Y. –Y. Noh, A. Facchetti, M. Caironi, *Adv. Funct. Mater.* 2014, **24**, 1151.
- [9] a) J. K. Lee, W. L. Ma, C. J. Brabec, J. S. Moon, J. Y. Kim, K. Lee, G. C. Bazan, A. J. Heeger, *J. Am. Chem. Soc.* 2008, **130**, 3619; b) S. J. Lou, J. M. Szarko, T. Xu, L. Yu, T. J. Marks and L. X. Chen, *J. Am. Chem. Soc.* 2011, **133**, 20661; c) X. Guo, C. Cui, M. Zhang, L. Huo, Y. Huang, J. Hou and Y. Li, *Energy Environ. Sci.* 2012, **5**, 7943; d) Y. Gu, C. Wang and T. P. Russell, *Adv. Energy Mater.* 2012, **2**, 683.
- [10] a) M. Wang, X. Hu, P. Liu, W. Li, X. Gong, F. Huang, Y. Cao, *J. Am. Chem. Soc.* 2011, **133**, 9638; b) J. Yuan, X. Huang, F. Zhang, J. Lu, Z. Zhai, C. Di, Z. Jiang, W. Ma, *J. Mater. Chem.* 2012, **22**, 22734.
- [11] a) L. Ye , Y. Jing , X. Guo , H. Sun , S. Q. Zhang , M. J. Zhang , L. J. Huo , J. H. Hou , *J. Phys. Chem. C* 2013, **117**, 14920 ; b) H. Q. Zhou , Y. Zhang , J. Seifter , S. D. Collins , C. Luo , G. C. Bazan , T.-Q. Nguyen , A. J. Heeger , *Adv. Mater.* 2013, **25**, 1646 .
- [12] a) C. Piliago, T. W. Holcombe, J. D. Douglas, C. H. Woo, P. M. Beaujuge, J. M. J. Fréchet, *J. Am. Chem. Soc.* 2010, **132**, 7595; b)
- [13] D. Qian, W. Ma, Z. Li, X. Guo, S. Zhang, L. Ye, H. Ade, Z. Tan, J. Hou, *J. Am. Chem. Soc.* 2013, **135**, 8464.

Toc: The number of conjugated side chains on the donor polymer can greatly affect the performance of all-polymer solar cells.



TOC



Scheme 1. Molecular structures and LUMO/HOMO energy levels of donor (P8, PT8 and PTP8) and acceptor (N2200) polymers investigated.

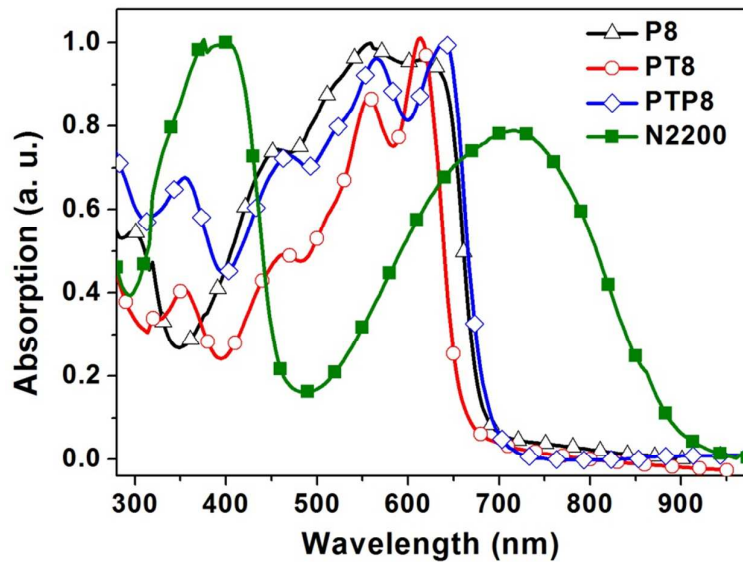


Figure 1. Normalized UV-vis. absorption spectra of donor and acceptor polymers in film spin-cast from chloroform.

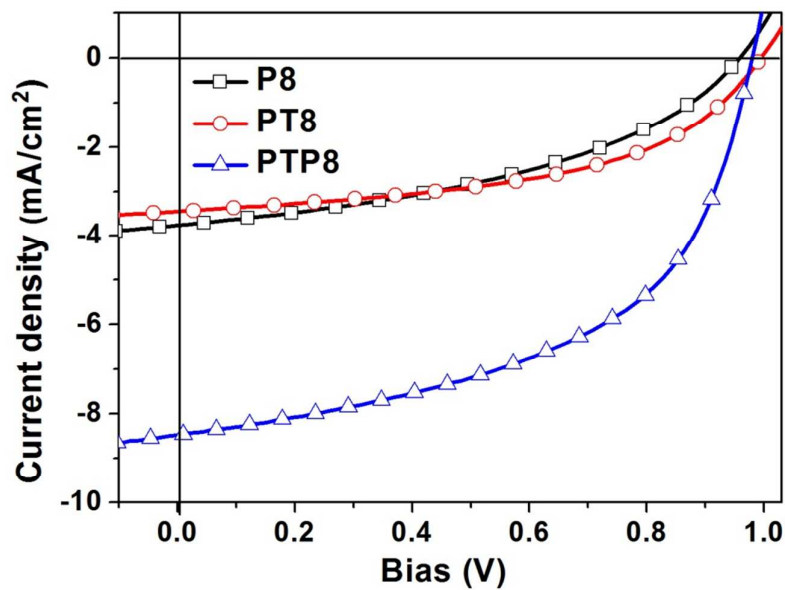


Figure 2. J - V curves of optimized all-polymer PSCs with different donor polymer and N2200.

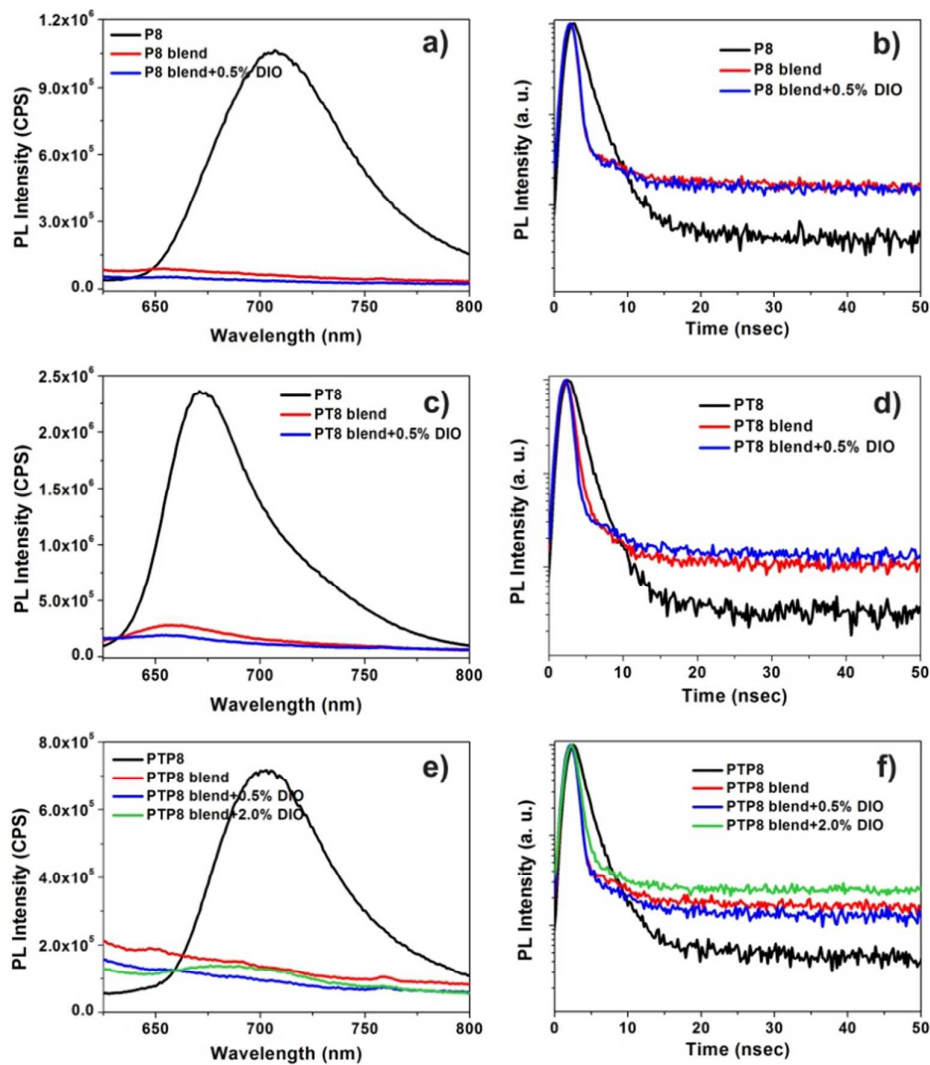


Figure 3. Photoluminescence spectra of polymer:N2200 based blend films (a, c, e); photoluminescence decay profiles of polymer:N2200 blend films (b, d, f).

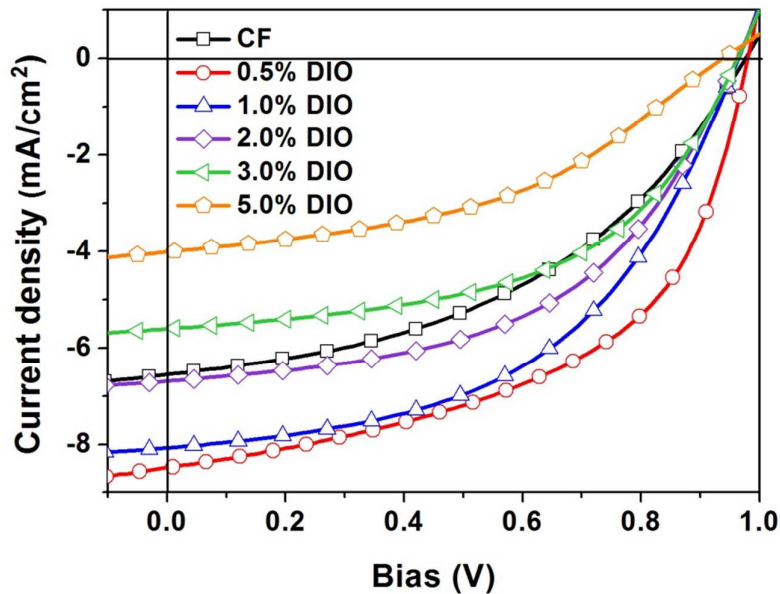


Figure 4. J - V curves of optimized all-polymer PSCs based on PTP8: N2200 with different DIO concentration,

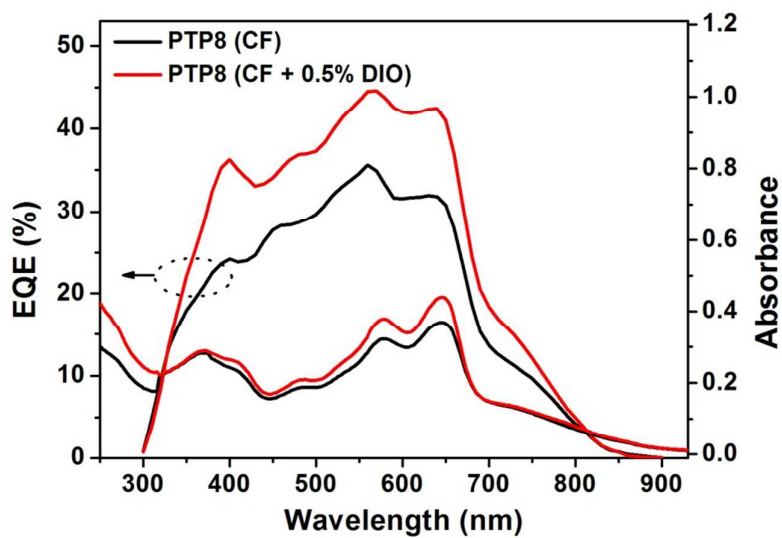


Figure 5. EQE and blend absorption spectra of PTP8:N2200 cast from chloroform w/wo solvent additive.

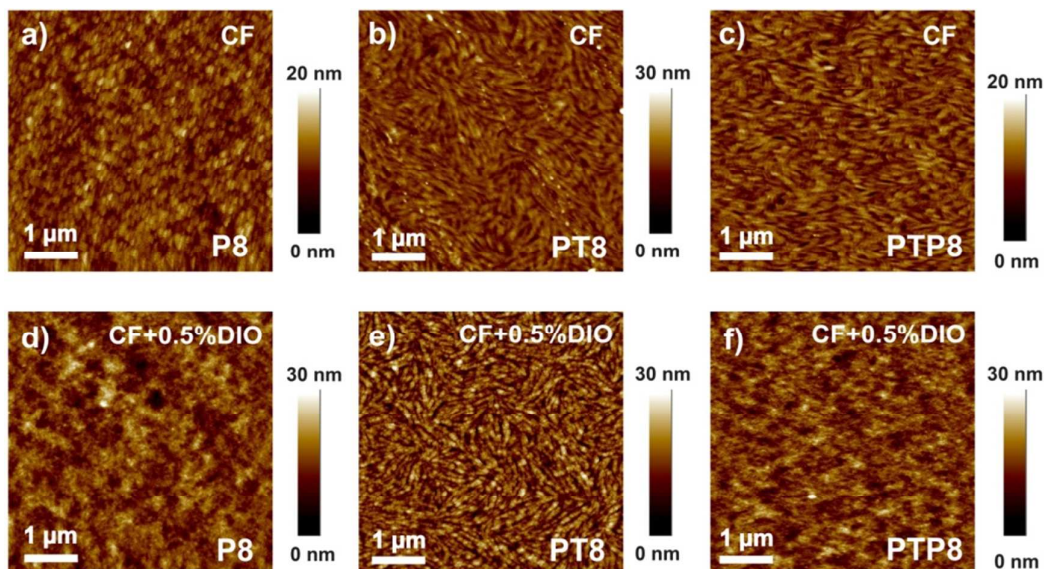


Figure 6. AFM height images ($5.0 \mu\text{m} \times 5.0 \mu\text{m}$) of polymer:N2200 blend films cast from chloroform w/w/o 0.5% (v/v) DIO.

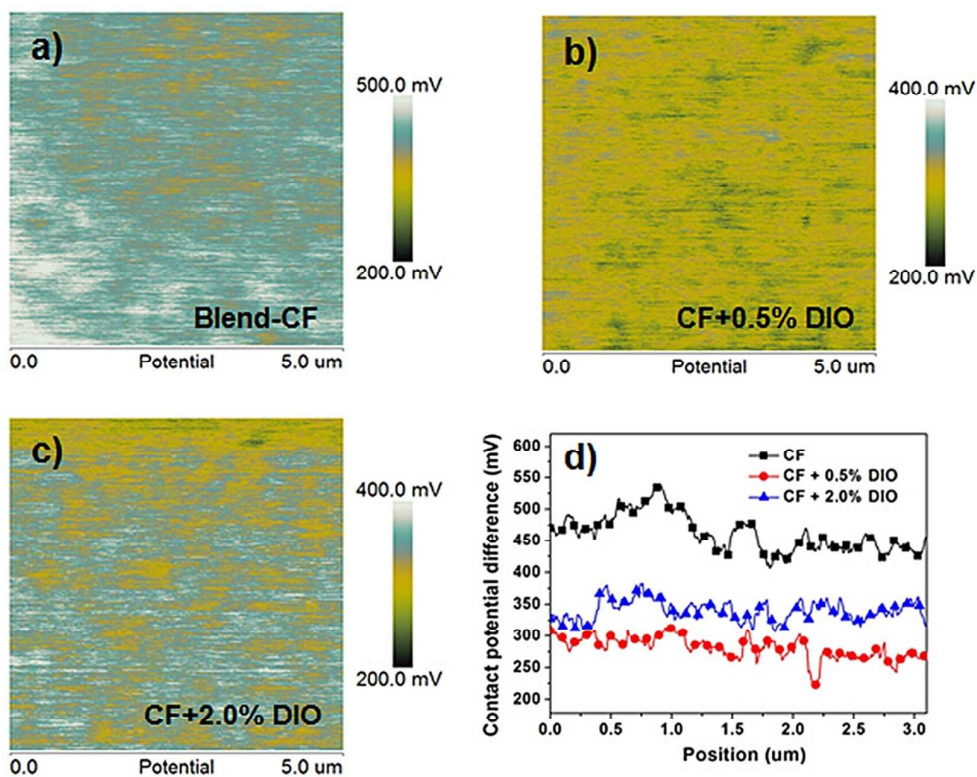


Figure 7. the PF-KPFM surface potential images ($5 \mu\text{m} \times 5 \mu\text{m}$) of PTP8: N2200 blend films and the analysis curves of the contact potential differences of the top surfaces for the blend films.

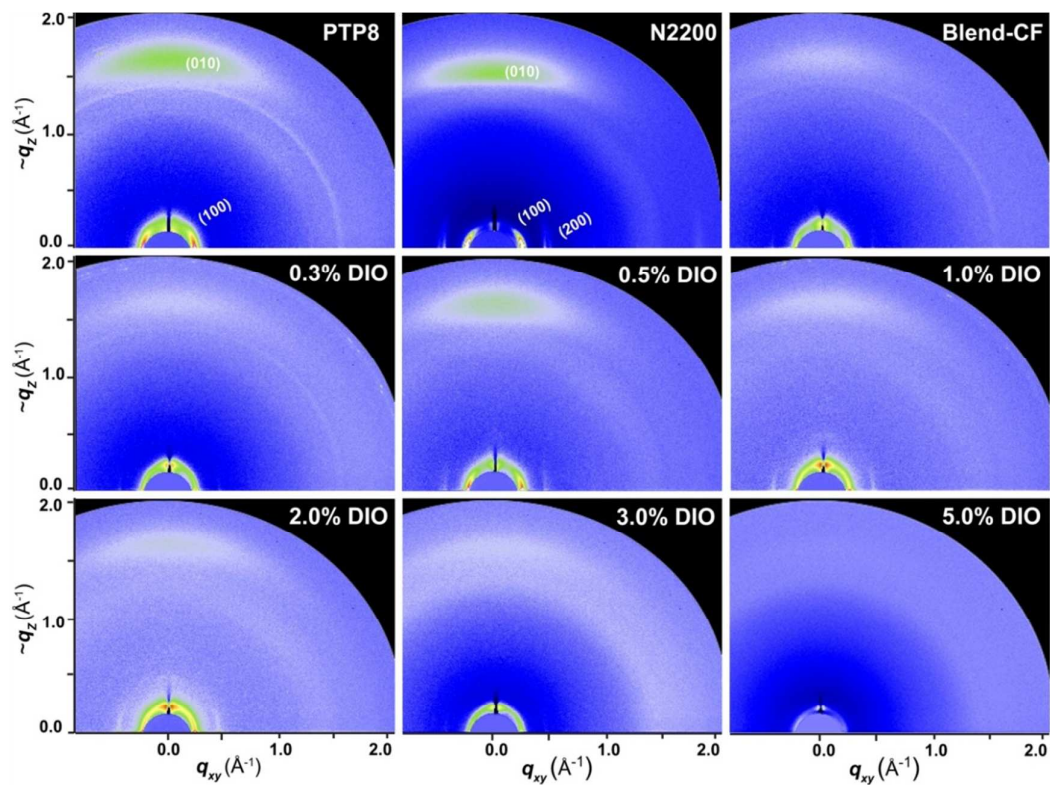


Figure 8. GIXD patterns of pristine PTP8 and N2200 film cast from chloroform as well as PTP8:N2200 blend films cast from chloroform with varying DIO concentration. Note that the 2D spectra have not been corrected for the “missing wedge” of data along the out-of-plane direction.

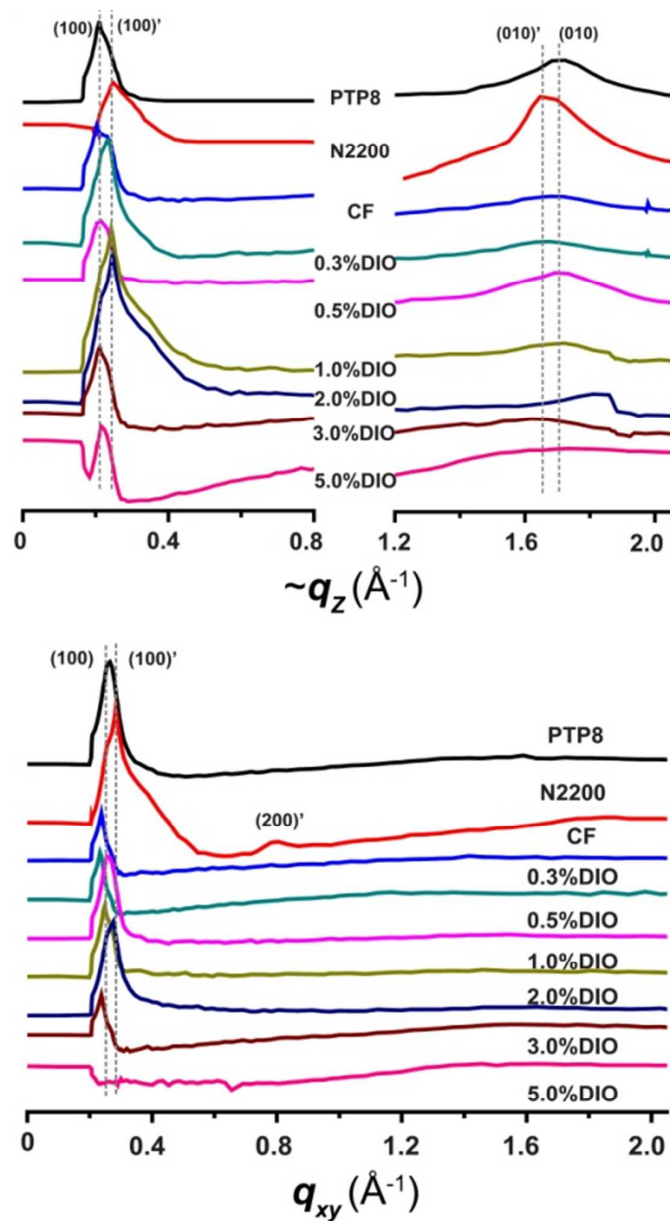


Figure 9. Out-of-plane and in-plane line cuts of 2D GIXD of PTP8 and N2200 as well as PTP8:N2200 blend film with different DIO concentration.

Table 1 Optimized Devices performance of PTP8:N2200 blend films cast from chloroform with varying DIO concentration.

	Additive	V_{oc} (V)	J_{sc} [mA/cm]	FF (%)	PCE (%) ^a
PTP8	None	0.975	6.53	44.4	2.83 (2.75 ± 0.08)
PTP8	0.5% DIO	0.978	8.43	52.8	4.35 (4.20 ± 0.15)
PTP8	1.0% DIO	0.960	8.05	50.2	3.88 (3.75 ± 0.13)
PTP8	2.0% DIO	0.960	6.67	51.1	3.27 (3.10 ± 0.17)
PTP8	3.0% DIO	0.962	5.59	52.5	2.82 (2.62 ± 0.20)
PTP8	5.0% DIO	0.938	4.00	43.8	1.64 (1.50 ± 0.14)

^a Averages values based on 6 parallel devices